Macromolecules

pubs.acs.org/Macromolecules Article

Polymer-Coupled Local Dynamics Enhances Conductivity of Ionic Liquids

Siqi Liu, Madhusudan Tyagi, and Pinar Akcora*

Cite This: *Macromolecules* 2020, 53, 6538−6546 Read Online

ACCESS | Metrics & More | Article Recommendations | Supporting Information

ABSTRACT: Solvent and polymer-grafted nanoparticle addition to 1-hexyl-3-methylimidazolium bis(trifluoromethylsulfonyl)imide (HMIM-TFSI) was investigated by measuring the translational diffusion of cationic species in quasi-elastic neutron scattering experiments and ionic conductivity by electrochemical impedance spectroscopy. Adding polymers or nanoparticles to neat ionic liquids generally increases their viscosity and lowers the ionic diffusivity. In this work, we added two different solvents (acetonitrile and methanol) to HMIM-TFSI/grafted particle mixtures to understand the interplay between polymer−ionic liquid interactions and conformational state of brushes, which governs the transport properties (diffusivity and conductivity) of ionic liquids. Our results showed that with grafted chains swollen in acetonitrile, the cationic mobility and ionic conductivity were improved with the number of grafted chains on particles. The unusual high diffusivity attained with the addition of PMMA-grafted magnetic nanoparticles suggests that polymer-coupled ionic liquid dynamics can be effective in increasing the free cation amount and, therefore, ionic conductivity in particle-based electrolytes.

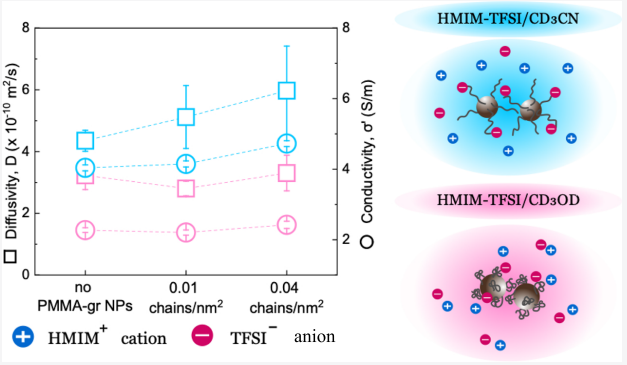

INTRODUCTION

Ionic liquids (ILs) are low-melting-point salts consisting of organic cations and organic/inorganic anions. They exhibit remarkable features like high ionic conductivity, broad electrochemical operation windows, negligible vapor pressure, and high thermal stability, which make them ideal candidates for electrochemical applications such as electrolytes in fuel cells,[1] batteries,[2] and separation membranes for the capture of carbon dioxide.[3−5] The inherent structural and dynamic heterogeneity in neat ILs have been investigated using both simulations[6,7] and experimental techniques of quasi-elastic neutron scattering,[8] neutron spin echo spectroscopy,[9] and X-ray scattering.[10] Transport properties of ILs are restricted by their high viscosity and low ion mobility, which limit their practical use in electrochemical devices. Mixtures of ILs,[11,12] small molecule or solvent addition[13,14] to ILs, are utilized to enhance the solvation and diffusivity of ILs and integral capacitance of supercapacitors. The effects of dipole moment, diffusivity, dielectric constant, viscosity, and composition of ILs on the supercapacitors' performance were evaluated in simulations,[13,14] using machine learning methods,[15] and experimentally by electrochemical impedance spectroscopy[16] and quasi-elastic neutron spectrometer[14] by adjusting dipole moments and compositions of IL mixtures.[12,14,17−19]

It is essential to understand the molecular interactions in IL/solvent mixtures as they determine the ionic association and solvation, which correlate to the ionic diffusion and conductivity. ILs with the smaller anion size generally have low binding energy between the ionic pairs and are known to exhibit faster ion transport.[20] Ionic dissociation occurs with organic solvents or water addition through hydrogen bonding interactions between the solvent and water,[21,22] and subsequently, molar conductivity increases with solvent content. The effect of alkyl chain length and anion type on ionic association has also been studied.[23] It was reported that increasing alkyl chain length of the imidazolium ring reduced the association of ILs in solvents due to the enhancement of solvation. On the other hand, results from both calculated molar conductivity[24] and simulated cation diffusivity[25] indicated that solvents with the higher dipole moments can better separate ions than the less polar solvents as a result of the weakened electrostatic interactions.

Among all the organic solvents discussed in the literature, acetonitrile is a very promising solvent to add into ILs for advanced electrolyte solution.[16,26,27] It was shown that acetonitrile interacts with the imidazolium ring through the

Received: June 18, 2020
Revised: July 7, 2020
Published: July 27, 2020

https://dx.doi.org/10.1021/acs.macromol.0c01434
Macromolecules 2020, 53, 6538−6546

$\pi-\pi$ interactions and with $TFSI^-$ anions through ion−dipole interactions.[28−31] Consequently, interactions between cations and anions are disrupted as acetonitrile dissociates the ion pairs.[28,32]

In this work, we introduced two different cosolvents, acetonitrile and methanol, to 1-hexyl-3-methylimidazolium bis(trifluormethylsulfonyl)imide (HMIM-TFSI) and measured the cation diffusivity and ionic conductivity with and without PMMA-grafted magnetic nanoparticles by quasi-elastic neutron scattering (QENS) and electrochemical impedance spectroscopy (EIS). Both acetonitrile and methanol can solvate HMIM-TFSI and interact with PMMA differently. This paper demonstrates the effect of polymer graft density on the solvation of ILs with the inclusion of acetonitrile and methanol. It is our intention that by probing the cation diffusion at short time and length scales, the ionic conductivity results can be explained beyond the solvent effect. We conjecture that the enhanced conductivity results with the highly swollen grafted chains in acetonitrile are due to the higher cation diffusivity since the mobility of cations is correlated with how anions interact with the polymer. The paper is structured to present the QENS results of IL/solvent mixtures to provide the convincing solvation effect of solvents. Next, the diffusivities of neat IL with PMMA-grafted particles at two grafting densities are presented, which are found to be similar. Dynamics data of IL/solvent mixtures with the grafted particles are then discussed with the ionic conductivity results. The diffusion and conductivity of ILs are shown to enhance with the incorporation of PMMA-grafted nanoparticles.

EXPERIMENTAL SECTION

Sample Preparation. Deuterated MMA (MMA-d_8, 98%) was purchased from Polymer Source, and 1-hexyl-3-methylimidazolium bis(trifluormethylsulf onyl)imide (HMIM-TFSI) was purchased from IoLitec (Ionic Liquids Technologies). Acetonitrile-d_3 (99.8 mol % D, CD_3CN) and methanol-d_4 (99.8 mol % D, CD_3OD) were purchased from Cambridge Isotope Laboratories, Inc. 4-Cyanopentanoic acid dithiobenzoate (CPDB), diethyl ether, oleic acid (90%), and oleylamine (70% technical grade) were purchased from Sigma-Aldrich. Tetrahydrofuran (THF) and cyclohexane (both ACS grades) were purchased from Pharmco-AAPER. 2,2′-Azobis(isobutyronitrile) (AIBN; 98% technical grade) was recrystallized from methanol. All other chemicals were used as received.

Nanoparticle Synthesis. Fe_3O_4 nanoparticles were synthesized by a high-temperature thermal decomposition method. The one-step reaction of nanoparticles utilizes iron(III)acetylacetonate ($Fe(acac)_3$) as a precursor and uses both oleic acid and oleylamine as surface ligands, which results in nanoparticles at high yields with no byproducts.[33] From the analysis of several transmission electron microscopy (TEM) images, the synthesized nanoparticles were found to be monodisperse with 6.4 ± 0.8 nm diameter.

Preparation of CPDB-Anchored Fe_3O_4 Nanoparticles. CPDB was added dropwise into a nanoparticle solution of 20 mg/mL and sonicated in a bath sonicator. The mixture was stirred at room temperature for 24 h. Particles were washed to remove excess CPDB following the previously reported protocol.[34] The mixture was precipitated by adding excess of cyclohexane and ethyl ether (4:1 volume ratio), centrifuged at 3000 rpm for 15 min, and redissolved in 25 mL of THF. The washing procedure was repeated three times.

Surface-Initiated Reversible Addition−Fragmentation Chain-Transfer Polymerization of Deuterated MMA from Fe_3O_4 Nanoparticles. CPDB-anchored Fe_3O_4 particles, deuterated MMA, and AIBN in THF solution were degassed in freeze−pump−thaw cycles. The flask was placed in an oil bath and stirred at 60 °C for 6 h. The flask was immersed in liquid nitrogen to terminate the polymerization via quenching. To purify the grafted particles, ethanol was added to the solution and centrifuged at 6000 rpm. The washing step was repeated several times till the supernatant solution was clear after ethanol addition. The supernatant was removed, and the particles were redissolved in THF. This procedure was repeated several times to remove the free PMMA chains.

Structural Characterization. TEM data were collected using an FEI TITAN THEMIS 200 TEM located at the CUNY-ASRC Imaging Facility operated at 200 kV. PMMA-grafted particles in ionic liquid solution were drop cast on lacey carbon grids. Samples for TEM are at lower particle concentrations compared to the samples for QENS.

Weight losses of polymer-grafted particles were measured using a thermogravimetric analyzer (Q50 TGA, TA Instruments). Nanoparticles were not etched to determine the molecular weight of deuterated PMMA due to limited amounts of grafted particles. Instead, we used the calibration curve to determine the grafting density and molecular weight of two batches of particles prepared for this work. Grafting density (σ) is calculated by the equation

$$\sigma = \frac{m_{\text{polymer}}}{m_{\text{NP}}}\frac{N_A \rho R}{3M_w} \tag{1}$$

where m_{polymer} and m_{NP} are the masses of grafted chains and particle core, respectively, N_A is the Avogadro constant, ρ is the particle density, R is the radius of iron oxide nanoparticles, and M_w is the weight-average molecular weight of grafted chains. Equation 1 is then arranged to

$$\frac{m_{\text{polymer}}}{m_{\text{NP}}} = \frac{\sigma}{M_w}\frac{3{M_w}^2}{N_A \rho R} + b \tag{2}$$

The mass ratio of grafted chains and core particles ($m_{\text{PMMA}}/m_{\text{NP}}$) was plotted versus the ratio of grafting density and molecular weight (σ/M_w) by compiling the data of particles with various graft densities lower than 0.2 chains/nm^2 collected in our laboratory over the years (Figure S1). The plotting factor (b) is applied in eq 2. Using the linear calibration line, the molecular weights of our two samples were determined. Equation 1 is then used to get σ. This calibration method was also used in our previous paper.[19]

Electrochemical Impedance Spectroscopy (EIS). Bulk ionic conductivity was measured using an SP-300 electrochemical impedance spectrometer from the Bio-Logic Science Instruments. Solutions (0.3 mL) of grafted particles in HMIM-TFSI/solvent mixtures (at 50/50 mass ratio) were placed into a tube with two stainless-steel electrodes. AC impedance measurements were performed at room temperature. An alternating current signal with 10 mV amplitude was applied in a frequency range of 1 kHz−1 MHz. The real component of the complex conductivity (σ') was calculated using the real (Z') and imaginary (Z'') parts of measured impedance according to the given equation[35] $\sigma'(\omega) = \frac{Z'(\omega)}{k[(Z'(\omega))^2 + (Z''(\omega))^2]}$. Figures S2 and S3 show the impedance and $\sigma'(\omega)$ data for all samples and for the neat IL and IL/solvent mixtures (Figure S4). The impedance spectra are dominated by ionic mobility at the high-frequency plateau,[36] and this value is used for the ionic conductivity of samples. The conductivity cell constant (k) was determined using a 0.01 M KCl standard (Ricca Chemical, 1412 μS/cm at 25 °C).

Quasi-Elastic Neutron Scattering (QENS). QENS experiments were performed using a high-flux backscattering spectrometer (HFBS, NG2) at the National Institute of Standards and Technology Center for Neutron Research (NCNR). A Si(111) monochromator with an incident neutron wavelength of 6.27 Å was used, providing an energy window of ±16 μeV with an energy resolution of ±0.8 μeV and a Q range at 0.25−1.75 Å^{-1}. QENS spectra were collected at 283 K for 13 h and kept in thermal equilibrium for 20 min at measurement temperature prior to data collection. Grafted particles at ∼1 mg/mL (2 wt%) concentration were mixed with pure HMIM-TFSI and mixtures of HMIM-TFSI/CD_3CN and HMIM-TFSI/CD_3OD at 50/50 mass ratio. Annular aluminum holders with 0.2−0.3 mm gaps were used to minimize multiple scattering. Indium wire was used to seal the sample holder effectively. The instrument resolution was measured

https://dx.doi.org/10.1021/acs.macromol.0c01434
Macromolecules 2020, 53, 6538−6546

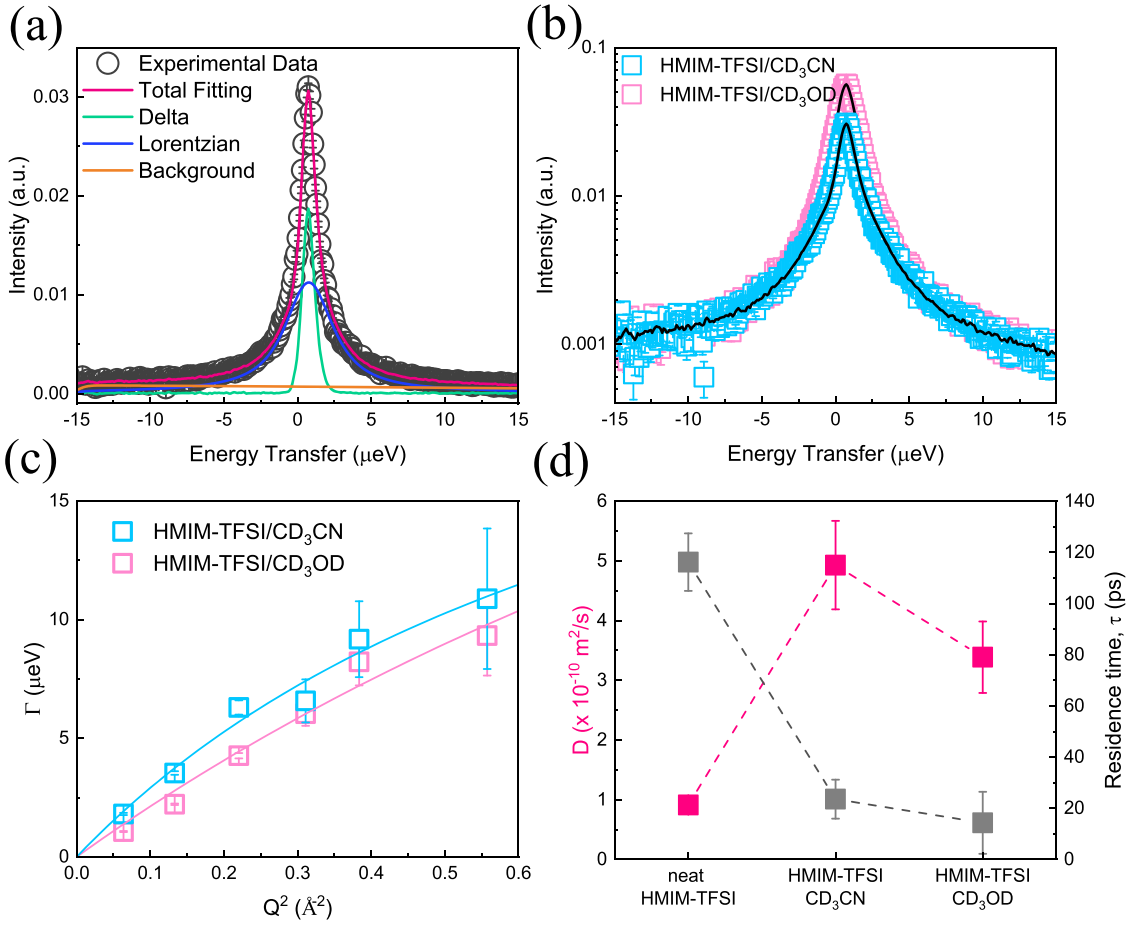

Figure 1. QENS data of HMIM-TFSI in different solvents. (a) Representative experimental QENS spectra for the HMIM-TFSI/CD_3OD mixture at Q = 0.252 $Å^{-1}$ fitted with delta function, single Lorentzian function, and linear background. (b) Experimental QENS spectra for HMIM-TFSI/CD_3CN and HMIM-TFSI/CD_3OD mixtures at 1:1 mass ratio. Black solid lines are the total fitting to the scattering data. (c) Jump diffusion model fit to the HWHM of QENS data of HMIM-TFSI/CD_3CN and HMIM-TFSI/CD_3OD mixtures. Error bars represent the standard deviation of Lorentzian fit. Solid lines show the jump diffusion model fits to the data. (d) Diffusivity and residence time of the $HMIM^+$ cation in neat HMIM-TFSI and HMIM-TFSI/CD_3CN and HMIM-TFSI/CD_3OD mixtures deduced from the jump diffusion model. Note that diffusivity and residence time for neat IL refer to the long-range (slow) translational diffusion measured using the BASIS at ORNL. Error bars represent one standard deviation throughout the text.

using a vanadium standard. The raw data were reduced and analyzed using a DAVE software package.[37]

RESULTS AND DISCUSSION

Solvation of ILs in organic solvents improves the transport properties by enhancing the diffusivity and ionic conductivity of ILs.[18] Thus, the high power density and energy density can be achieved with the solvation of IL, which find uses in various electrochemical devices. Electrochemical impedance spectroscopy (EIS) measures the ionic conductivity from all charged species, and it is commonly used to investigate the effect of solvent association on ILs' transport properties.[21,24,38] Pulsed-gradient spin echo nuclear magnetic resonance spectroscopy (PGSE-NMR) measures the time-averaged diffusivity of cations or anions in dilute systems. The molar conductivity (Λ) is calculated using the Nernst−Einstein equation: $\Lambda = \frac{Ne^2}{kT}(D_+ + D_-)$, where D_+ and D_- are the diffusivities of cations and anions, respectively, N is the Avogadro number, and e is the electric charge on the ionic carrier.[18,22,38] The molar conductivity generally overestimates the actual conductivity of the system because of ion aggregation in pure IL or IL/solvent or IL/polymer mixtures.[21,39−41]

High ionic diffusivities and maximum ionic conductivities were observed at intermediate IL/solvent concentrations.[18,25] Our recent results again confirmed that ionic conductivities reached maxima at equimass compositions of IL and solvent with varying polarities.[42] The improved conductivity results of IL are purely explained by solvation of the ionic pairs with the addition of polar solvents that can weaken the cation−anion interactions. IL diffusivity in polar solvents was also found to be strongly correlated with high solvent concentrations.[18] In this study, polymer-grafted nanoparticles in HMIM-TFSI/acetonitrile and HMIM-TFSI/methanol mixtures at equal mass concentrations were prepared to measure the cation ($HMIM^+$) diffusion characteristics at small length scales (~1 nm) in QENS. EIS experiments were conducted to reveal how addition of grafted chains and solubility of the polymer in the solvent affects the ionic conductivities of HMIM-TFSI.

QENS measures the translational diffusion and diffusive-like dynamics on the length scale of fractions of a nanometer and the time scale of a few nanoseconds to picoseconds.[43] QENS is sensitive to isotopes with large incoherent neutron scattering cross sections. The incoherent scattering, coherent scattering, and absorption cross sections of all species used in this work

https://dx.doi.org/10.1021/acs.macromol.0c01434
Macromolecules 2020, 53, 6538−6546

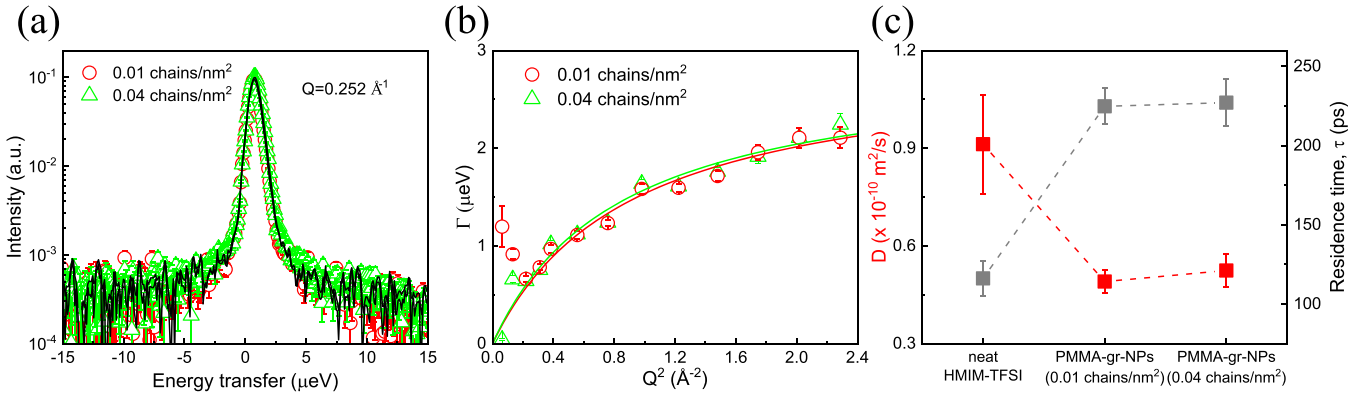

Figure 2. QENS data of HMIM-TFSI with polymer-grafted nanoparticles. (a) QENS spectra for HMIM-TFSI with PMMA-grafted nanoparticles with two grafting densities of 0.01 and 0.04 chains/nm^2 at $Q = 0.252$ Å^{-1}. The grafted particle concentration is 2 wt % in both solutions. Black solid lines are the total fitting to the scattering data. (b) Jump diffusion model fits to the HWHM of QENS data of PMMA-grafted nanoparticles in HMIM-TFSI. Error bars are the standard deviation of Lorentzian fits. Solid lines show the jump diffusion model fits. (c) Diffusivity and characteristic residence time of neat HMIM-TFSI (from ref 19) and PMMA-grafted particles of 0.01 and 0.04 chains/nm^2 in HMIM-TFSI.

are given in Table S1. The low incoherent signals from Fe_3O_4 nanoparticles and deuterated PMMA allow us to probe the incoherent scattering from the hydrogens of the $HMIM^+$ cations only in QENS since there is no hydrogen in the $TFSI^-$ anion. The effect of cosolvents, deuterated acetonitrile (CD_3CN) and deuterated methanol (CD_3OD), on cation ($HMIM^+$) dynamics is presented with the QENS data. We will use IL for HMIM-TFSI in the rest of the paper. The scattering from the $HMIM^+$ cation is reduced following the reduction protocol used in QENS experiments simply by implementing the below equation

$$I_{IL}(Q, E) = [X(Q)\delta(E) + (1 - X(Q))S(Q, E)]\circledast R(Q, E) + B(Q, E) \quad (3)$$

$X(Q)$ represents the fraction of elastic scattering, $\delta(E)$ is the delta function for the elastic contribution to the measured spectra, and $(1 - X(Q))$ is the quasi-elastic component of QENS contributing to the overall scattering intensity. $S(Q, E)$ is the dynamic structure factor, $R(Q, E)$ is the instrument resolution function, and $B(Q, E)$ is the linear background term. $S(Q, E)$ is fitted to a single Lorentzian function as shown in the following:

$$S(Q, E) = \frac{1}{\pi}\frac{\Gamma(Q)}{\Gamma(Q)^2 + E^2} \quad (4)$$

where $\Gamma(Q)$ represents the broadening of the $S(Q, E)$ functions in terms of half widths at half-maxima (HWHM) of the Lorentzian function. The total fittings of delta and single Lorentzian functions and linear background on a representative QENS spectrum are shown in Figure 1a for HMIM-TFSI/CD_3CN at $Q = 0.252$ Å^{-1}. Figure 1b shows the higher intensity at zero energy transfer in IL/CD_3OD compared to IL/CD_3CN in the QENS spectra, which is due to the slightly higher IL mole fraction (93 mol %) in CD_3OD solution than in CD_3CN (91 mol %). The broadening of the QENS spectrum represents fast translational diffusion. It is clearly seen that IL/CD_3CN has higher broadening than the IL/CD_3OD within a Q range from 0.25 to 0.75 Å^{-1} (Figure 1c), resulting from enhancement of diffusion mobility. The data between $Q = 0.75$ and $Q = 1.75$ Å^{-1} were ignored for samples containing solvents as the dynamic process in such a small length scale is very fast and shorter than time windows of HFBS. Future experiments are planned in disk chopper spectroscopy to investigate the cation diffusion at a higher Q range. Figure 1c shows the Q^2-dependence of HWHM and fits with the jump diffusion model, originally proposed by Singwi and Sjölander[44] with the given equation

$$\Gamma(Q) = \frac{\hbar D Q^2}{1 + DQ^2\tau} \quad (5)$$

Here, D is the diffusion coefficient, τ is the characteristic residence time, *i.e.*, the average time that a particle spends at a site before moving rapidly (jumping) to another site, $\hbar$ is the reduced Planck's constant, and Q is the scattering vector. Unlike Brownian motion that is valid for continuous motions, the jump diffusion model describes translational motion with concrete events and exponentially distributed jump lengths.[44] The residence time can serve as a measure of the time between proton transfer events.[45] The diffusivity (D) and characteristic residence time (τ) of $HMIM^+$ cations in two solutions and the neat IL are plotted in Figure 1d. The neat IL was measured using a BASIS backscattering spectrometer at Oak Ridge National Laboratory (ORNL), and its dynamic structure factor was fitted with a sum of two Lorentzian functions to deduce slow and fast diffusion processes.[19] The slow dynamics corresponds to the long-range unrestricted diffusion, and the slow dynamics is presented in Figure 1d. With addition of the solvent (either acetonitrile or methanol), the diffusivity was increased by a factor of 4, as shown in Figure 1d. The residence time correspondingly decreased with higher diffusion mobility. This result is consistent with the previously reported QENS results on the enhanced diffusivity of cations in solvents with high dipole moments.[25] It was shown that the $BMIM^+$ cation exhibited the increased mobility when mixed with acetonitrile (an apolar solvent) compared with methanol (a polar solvent).[25] The higher diffusivity of the $BMIM^+$ cation than the $HMIM^+$ cation in the same solvent mixtures was attributed to the lower viscosity of BMIM-TFSI (51 mPa·s)[46] compared to HMIM-TFSI (70.09 mPa·s)[47] and different dynamic ranges and energy resolutions of the two QENS instruments.

PMMA can be solvated with 1-ethyl-3-methylimidazolium bis(trifluoromethylsulfonyl)imide (EMIM-TFSI) and interacts with the $TFSI^-$ anion, prohibiting the formation of ion clusters.[48] The increase in the number of ion carriers indicated that PMMA can promote the ion dissociation between $EMIM^+$

https://dx.doi.org/10.1021/acs.macromol.0c01434
Macromolecules 2020, 53, 6538−6546

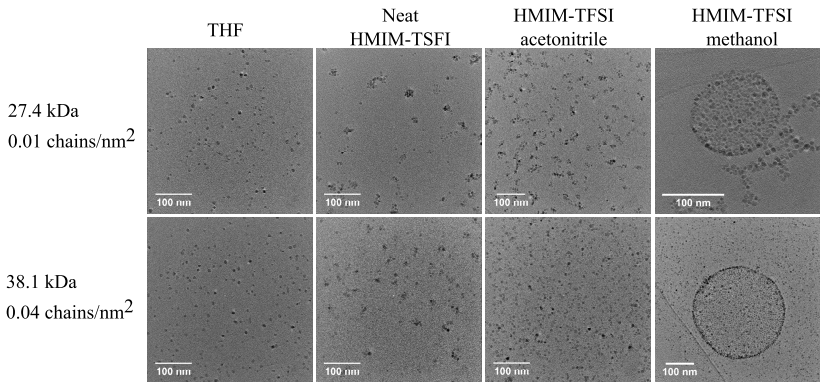

Figure 3. TEM micrographs of PMMA-grafted particle solvent cast from THF, neat HMIM-TFSI, and HMIM-TFSI/acetonitrile and HMIM-TFSI/methanol mixtures.

and the $TFSI^-$ anion.[48] Two relaxation processes of $EMIM^+$ probed in the PMMA ion gel system[49] were attributed to the diffusion of free ions in bulk EMIM-TFSI and to the ions that were bound to PMMA. Coulombic interactions between PMMA and the $TFSI^-$ anion of HMIM-TFSI can dissociate the HMIM-TFSI and hence increase the number of free cations.[19] Subsequently, the enhanced long-range unrestricted diffusion of $HMIM^+$ cations in well-dispersed grafted nanoparticles was measured in QENS.[19] Other works with PMMA-grafted nanoparticles in imidazolium-based IL shows the good stabilization of particles by DLS (dynamic light scattering) and TEM.[50−52]

It is expected that the swelling of PMMA brushes with IL depends on the grafting density and chain length. We synthesized deuterated PMMA (27.4 and 38.1 kDa)-grafted iron oxide nanoparticles with 0.01 and 0.04 chains/nm^2 graft densities. The QENS spectra of the two grafted samples (2 wt % in HMIM-TFSI) overlapped well within the whole energy transfer range at a representative Q value of 0.252 $Å^{-1}$, as seen in Figure 2a. The raw data suggest that the translational diffusion of $HMIM^+$ cations is almost identical with particles at different graft densities. The Q^2-dependent HWHM of Lorentzian functions in Figure 2b represent the similar mobility. The residence times of cations are higher than those of the neat HMIM-TFSI, and correspondingly, their diffusivity is smaller, as seen in Figure 2c. This slowing down in mobility was attributed to the viscosity increase with the addition of grafted particles. Simply, adding nonconducting polymer-grafted particles lowers the diffusivity of ionic liquids only slightly because of the low particle concentration in IL.

Knowing that solvent polarity and solvent diffusivity enhance the ion mobility,[42] next we studied how solvent addition contributes to the fast dynamics of IL containing PMMA-grafted particles in QENS. Dynamic light scattering results of grafted particles in IL/acetonitrile and IL/methanol mixtures showed that particles agglomerated due to weak solubility of PMMA in methanol and they well dispersed in acetonitrile as a result of good solubility of PMMA in acetonitrile.[42] The miscibility of PMMA-grafted particles in acetonitrile and methanol is supported by TEM data, as shown with well dispersion in neat IL and IL/acetonitrile mixture for both grafting densities (Figure 3). The phase segregation of particles suggests the limited interactions between the IL and polymer. The solvation effect induced by ion−dipolar interactions between PMMA−IL and IL−solvent has been previously observed by ionic conductivities in our previous work.[42] With the QENS results discussed below, we underpin how polymer-coupled anions facilitate the cation dynamics of IL.

QENS spectra of IL/CD_3CN and IL/CD_3OD mixtures with two different PMMA-grafted particles are presented in Figure 4a,c. The slight decrease in HWHM of the IL/CD_3CN and IL/CD_3OD mixtures after adding grafted particles suggests the slowing down in dynamics of IL (Figure 4b,d). However, the cation diffusivities obtained from the jump diffusion model indicate faster dynamics with the particles in CD_3CN, as shown in Figure 4e. Residence times in both solvents indicate that IL dynamics slowed down with particle addition in both solvents (Table S2). The larger residence times for the IL/CD_3CN with particles than the neat IL/CD_3CN and also than the particles in CD_3OD are in line with the raw data (Figure 4b,d) but are not consistent with diffusivity results. This is because the ions can reside at longer times between two jumps but still can diffuse faster.

Acetonitrile (CD_3CN) was added to decrease the viscosity and hence to enhance the transport of ionic species. CD_3CN is a good solvent for PMMA and miscible with ILs.[29−31,53] The IL containing the high graft density (0.04 chains/nm^2) particles has higher diffusivity than the IL with the low graft density (0.01 chains/nm^2) particles. This interesting finding reveals that the number of PMMA chains interacting with $TFSI^-$ anions increased the number of the free $HMIM^+$ cations and their diffusivity. The polymer-coupled anion and increased diffusion of cation carriers were shown in our previous study,[19] but here, we present the grafting density and solvation effect on cation mobilities. In methanol, PMMA chains are in collapsed states, so mixing of IL and PMMA is limited and a decrease in cation diffusivity is observed. We conjecture that the lower interaction between PMMA and IL/methanol does not contribute to solvation of IL with PMMA, and thus diffusivity of IL remains almost the same for both grafted particles in methanol.

The conductivities of all samples are presented in Figure 5a. We found that the ionic conductivity trend is consistent with the cation diffusivity results. Conductivity was measured to be higher in IL/CD_3CN for both grafting densities, and the higher grafting density particles exhibited the higher conductivity in both CD_3CN and CD_3OD. While the solvent solvated the IL, the swelling state of brushes also dictated the solvation process, thereby increased the preferential ion−dipole interactions between the anions and PMMA (Scheme S1). The IL was solvated by CD_3OD at a lesser extent, and the grafted polymer

https://dx.doi.org/10.1021/acs.macromol.0c01434
Macromolecules 2020, 53, 6538−6546

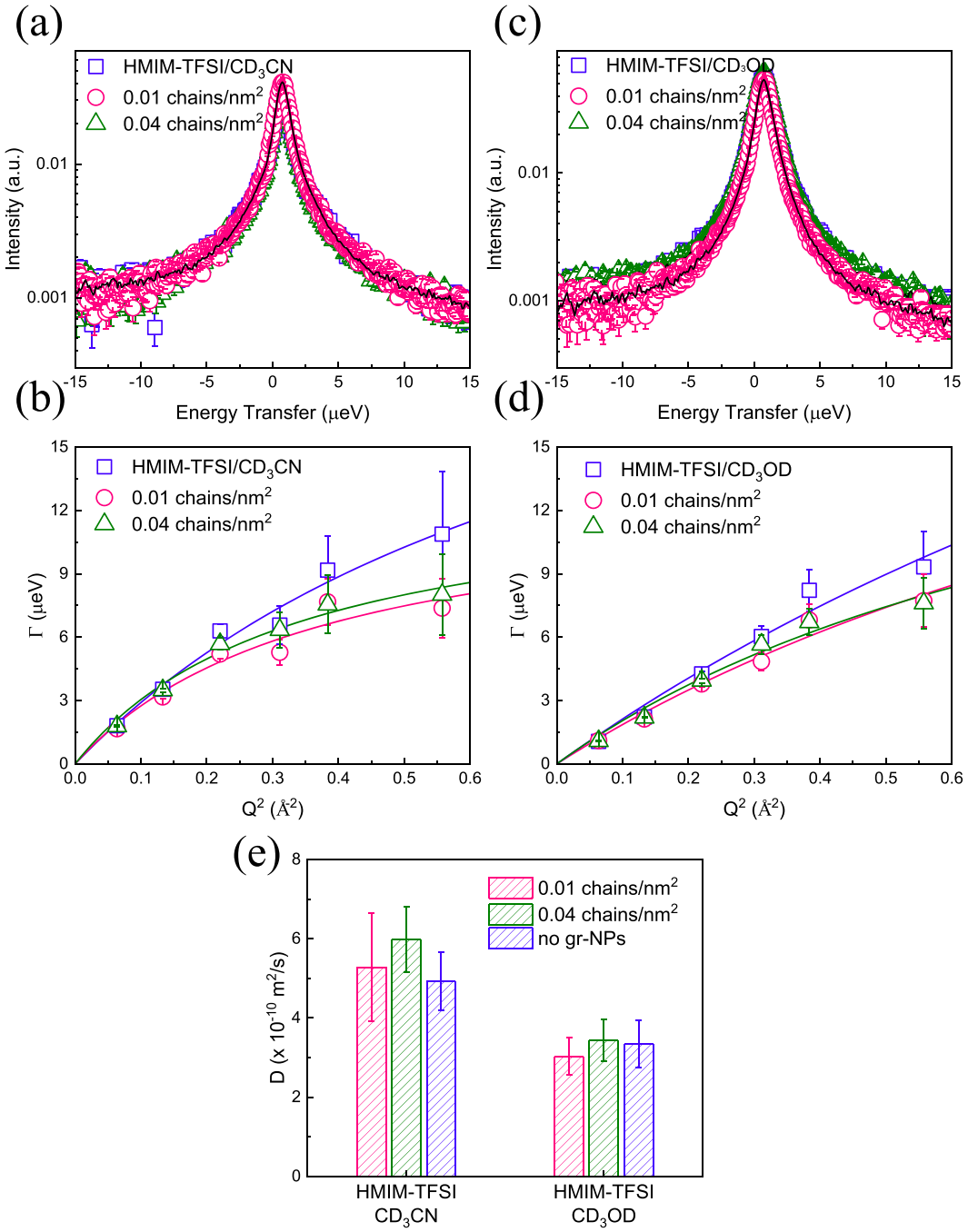

Figure 4. QENS data of HMIM-TFSI in the presence of grafted nanoparticles with two different solvents. (a) QENS spectra at $Q = 0.252$ Å^{-1} of PMMA-grafted nanoparticles with 0.01 and 0.04 chains/nm^2 in HMIM-TFSI/CD_3CN. (b) Quadratic dependence of HWHM from Lorentzian broadening of HMIM-TFSI/CD_3CN samples. (c) HMIM-TFSI/CD_3OD and PMMA-grafted nanoparticles with 0.01 and 0.04 chains/nm^2 in HMIM-TFSI/CD_3OD and (d) their HWHM fittings to the jump diffusion model. (e) Diffusivities deduced from the jump diffusion model fits for all samples. The grafted particle concentration is ∼1 mg/mL (2 wt %), and the mass ratio of HMIM-TFSI/CD_3CN and HMIM-TFSI/CD_3OD is 50/50.

shrunk to minimize interfacial energy.[25] As a result of both factors, conductivity decreased. Figure 5b shows the deviation of the normalized conductivity for two grafting density particles in both solvents. The conductivity of samples, grafted particles in IL/solvent, was normalized by the conductivity of IL/solvent solutions, $\sigma'/(\phi\sigma'_{IL/solvent})$, where ϕ and $\sigma'_{IL/solvent}$ are the volume fraction and conductivity of IL/solvent, respectively. An increase of 5−20% in conductivity of the IL/CD_3CN mixture with the addition of particles is attributed to the small concentration of particles in mixtures.

CONCLUSIONS

In this work, we focus on how polymer/solvent and ionic liquid/solvent interactions influence the cation mobility and ionic conductivity of HMIM-TFSI. We systematically measured the cationic mobility of HMIM-TFSI/solvent and of the same solutions with PMMA-grafted nanoparticles in QENS experiments. The solvent addition to neat HMIM-TFSI enhanced the diffusivity of $HMIM^+$ cations as a result of solvation. The unusual fast mobility of cations is observed for

https://dx.doi.org/10.1021/acs.macromol.0c01434
Macromolecules 2020, 53, 6538−6546

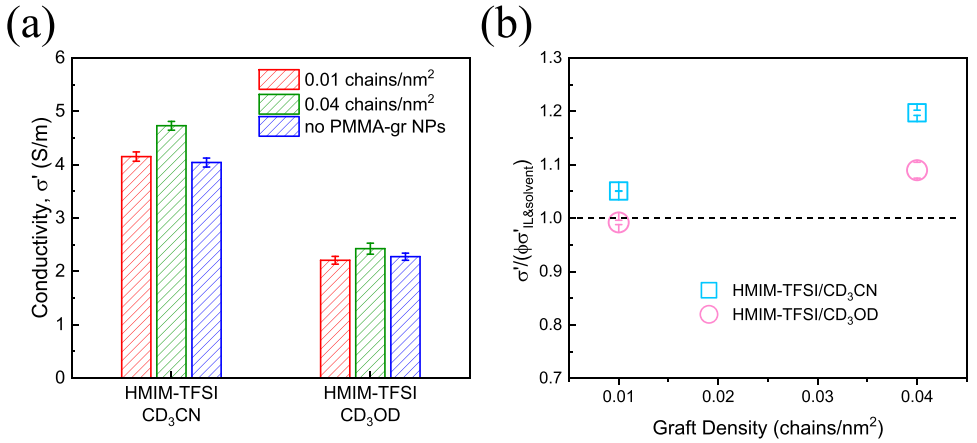

Figure 5. Comparison of ionic conductivities of PMMA-grafted nanoparticles in HMIM-TFSI/solvent and in neat HMIM-TFSI. (a) 27.4 kDa PMMA at 0.01 chains/nm^2 and 38.2 kDa PMMA at 0.04 chains/nm^2 in HMIM-CD_3CN and HMIM-CD_3OD. (b) Normalized conductivity data showing the contribution of PMMA-grafted particles to the enhanced conductivity.

HMIM-TFSI containing high grafting density particles. The cationic mobility and ionic conductivity results are explained by the conformational state of brushes in good and bad solvents. Particles with higher density graft chains offer more PMMA chains that can interact with $TFSI^-$ anions, and thus the increased number of free $HMIM^+$ cations leads to faster ion mobility in HMIM-TFSI/acetonitrile mixtures. The poor solubility of PMMA in methanol hinders the transport properties and solvation of HMIM-TFSI. This study demonstrates that the conductivity and mobility of ionic species of HMIM-TFSI can be improved by incorporating the PMMA-grafted particles into HMIM-TFSI at a minimal amount. It is anticipated that transport properties of ionic liquids can be further enhanced with high loadings and with the dispersion state of grafted particles.

■ ASSOCIATED CONTENT

Supporting Information

The Supporting Information is available free of charge at https://pubs.acs.org/doi/10.1021/acs.macromol.0c01434.

Coherent and incoherent neutron scattering cross sections, characteristic residence times of PMMA-grafted particles in IL/solvent mixtures, impedance−frequency plot, weight loss-grafting density calibration line, and illustration of anion−dipole interactions between $TFSI^-$ and PMMA (PDF)

■ AUTHOR INFORMATION

Corresponding Author

Pinar Akcora − *Department of Chemical Engineering & Materials Science, Stevens Institute of Technology, Hoboken, New Jersey 07030, United States;* orcid.org/0000-0001-7853-7201; Phone: (201) 216-5060; Email: pakcora@stevens.edu

Authors

Siqi Liu − *Department of Chemical Engineering & Materials Science, Stevens Institute of Technology, Hoboken, New Jersey 07030, United States*

Madhusudan Tyagi − *NIST Center for Neutron Research, Gaithersburg, Maryland 20899, United States; Department of Materials Science and Engineering, University of Maryland, College Park, Maryland 20742, United States*

Complete contact information is available at: https://pubs.acs.org/10.1021/acs.macromol.0c01434

Author Contributions

The manuscript was written through contributions of all authors. All authors have given approval to the final version of the manuscript.

Notes

The authors declare no competing financial interest.

■ ACKNOWLEDGMENTS

This work was supported by the National Science Foundation DMR Polymers program under award #1807802. Access to the HFBS was provided by the Center for High-Resolution Neutron Scattering, a partnership between the NIST and the NSF under agreement no. DMR-1508249. Certain commercial equipment, instruments, or materials are identified in this paper in order to specify the experimental procedure adequately. Such identification is not intended to imply recommendation or endorsement by the NIST. The authors would like to acknowledge the Imaging Facility of CUNY Advanced Science Research Center for instrument use, scientific and technical assistance.

■ REFERENCES

(1) Díaz, M.; Ortiz, A.; Ortiz, I. Progress in the Use of Ionic Liquids as Electrolyte Membranes in Fuel Cells. *J. Membr. Sci.* **2014**, *469*, 379−396.

(2) Xu, K. Nonaqueous Liquid Electrolytes for Lithium-Based Rechargeable Batteries. *Chem. Rev.* **2004**, *104*, 4303−4418.

(3) Yang, Z.-Z.; Zhao, Y.-N.; He, L.-N. CO2 Chemistry: Task-Specific Ionic Liquids for CO2 Capture/Activation and Subsequent Conversion. *RSC Adv.* **2011**, *1*, 545−567.

(4) Dai, Z.; Noble, R. D.; Gin, D. L.; Zhang, X.; Deng, L. Combination of Ionic Liquids with Membrane Technology: A New Approach for CO2 Separation. *J. Membr. Sci.* **2016**, *497*, 1−20.

(5) Bara, J. E.; Camper, D. E.; Gin, D. L.; Noble, R. D. Room-Temperature Ionic Liquids and Composite Materials: Platform Technologies for CO2 Capture. *Acc. Chem. Res.* **2010**, *43*, 152−159.

(6) Aoun, B.; Goldbach, A.; González, M. A.; Kohara, S.; Price, D. L.; Saboungi, M.-L. Nanoscale Heterogeneity in Alkyl-methylimidazolium Bromide Ionic Liquids. *J. Chem. Phys.* **2011**, *134*, 104509.

(7) Triolo, A.; Russina, O.; Bleif, H.-J.; Di Cola, E. Nanoscale Segregation in Room Temperature Ionic Liquids. *J. Phys. Chem. B* **2007**, *111*, 4641−4644.

(8) Kofu, M.; Tyagi, M.; Inamura, Y.; Miyazaki, K.; Yamamuro, O. Quasielastic Neutron Scattering Studies on Glass-Forming Ionic Liquids with Imidazolium Cations. *J. Chem. Phys.* **2015**, *143*, 234502.
(9) Kofu, M.; Nagao, M.; Ueki, T.; Kitazawa, Y.; Nakamura, Y.; Sawamura, S.; Watanabe, M.; Yamamuro, O. Heterogeneous Slow Dynamics of Imidazolium-Based Ionic Liquids Studied by Neutron Spin Echo. *J. Phys. Chem. B* **2013**, *117*, 2773−2781.
(10) Russina, O.; Triolo, A.; Gontrani, L.; Caminiti, R. Mesoscopic Structural Heterogeneities in Room-Temperature Ionic Liquids. *J. Phys. Chem. Lett.* **2012**, *3*, 27−33.
(11) Dhakal, P.; Shah, J. K. Recent Advances in Molecular Simulations of Ionic Liquid−Ionic Liquid Mixtures. *Curr. Opin. Green Sustain. Chem.* **2019**, *18*, 90−97.
(12) Lian, C.; Liu, K.; Van Aken, K. L.; Gogotsi, Y.; Wesolowski, D. J.; Liu, H. L.; Jiang, D. E.; Wu, J. Z. Enhancing the Capacitive Performance of Electric Double-Layer Capacitors with Ionic Liquid Mixtures. *ACS Energy Lett.* **2016**, *1*, 21−26.
(13) Liu, K.; Wu, J. Boosting the Performance of Ionic-Liquid-Based Supercapacitors with Polar Additives. *J. Phys. Chem. C* **2016**, *120*, 24041−24047.
(14) Osti, N. C.; Matsumoto, R. A.; Thompson, M. W.; Cummings, P. T.; Tyagi, M.; Mamontov, E. Microscopic Dynamics in an Ionic Liquid Augmented with Organic Solvents. *J. Phys. Chem. C* **2019**, *123*, 19354−19361.
(15) Su, H.; Lian, C.; Liu, J.; Liu, H. Machine Learning Models for Solvent Effects on Electric Double Layer Capacitance. *Chem. Eng. Sci.* **2019**, *202*, 186−193.
(16) Zhang, Q.; Liu, X.; Yin, L.; Chen, P.; Wang, Y.; Yan, T. Electrochemical Impedance Spectroscopy on the Capacitance of Ionic Liquid−Acetonitrile Electrolytes. *Electrochim. Acta* **2018**, *270*, 352−362.
(17) Jiang, D.-E.; Wu, J. Unusual Effects of Solvent Polarity on Capacitance for Organic Electrolytes in a Nanoporous Electrode. *Nanoscale* **2014**, *6*, 5545−5550.
(18) Thompson, M. W.; Matsumoto, R.; Sacci, R. L.; Sanders, N. C.; Cummings, P. T. Scalable Screening of Soft Matter: A Case Study of Mixtures of Ionic Liquids and Organic Solvents. *J. Phys. Chem. B* **2019**, *123*, 1340−1347.
(19) Liu, S.; Liedel, C.; Tarakina, N. V.; Osti, N. C.; Akcora, P. Dynamics of Ionic Liquids in the Presence of Polymer-Grafted Nanoparticles. *Nanoscale* **2019**, *11*, 19832−19841.
(20) Borodin, O.; Gorecki, W.; Smith, G. D.; Armand, M. Molecular Dynamics Simulation and Pulsed-Field Gradient NMR Studies of Bis(fluorosulfonyl)imide (FSI) and Bis[(trifluoromethyl)sulfonyl]-imide (TFSI)-Based Ionic Liquids. *J. Phys. Chem. B* **2010**, *114*, 6786−6798.
(21) Li, W.; Zhang, Z.; Han, B.; Hu, S.; Xie, Y.; Yang, G. Effect of Water and Organic Solvents on the Ionic Dissociation of Ionic Liquids. *J. Phys. Chem. B* **2007**, *111*, 6452−6456.
(22) Tokuda, H.; Baek, S.-J.; Watanabe, M. Room-Temperature Ionic Liquid-Organic Solvent Mixtures: Conductivity and Ionic Association. *Electrochemistry* **2005**, *73*, 620−622.
(23) Wang, H.; Wang, J.; Zhang, S.; Pei, Y.; Zhuo, K. Ionic Association of the Ionic Liquids [C4mim][BF4], [C4mim][PF6], and [Cnmim]Br in Molecular Solvents. *ChemPhysChem* **2009**, *10*, 2516−2523.
(24) Fox, E. T.; Paillard, E.; Borodin, O.; Henderson, W. A. Physicochemical Properties of Binary Ionic Liquid−Aprotic Solvent Electrolyte Mixtures. *J. Phys. Chem. C* **2013**, *117*, 78−84.
(25) Osti, N. C.; Van Aken, K. L.; Thompson, M. W.; Tiet, F.; Jiang, D.-E.; Cummings, P. T.; Gogotsi, Y.; Mamontov, E. Solvent Polarity Governs Ion Interactions and Transport in a Solvated Room-Temperature Ionic Liquid. *J. Phys. Chem. Lett.* **2017**, *8*, 167−171.
(26) Timperman, L.; Skowron, P.; Boisset, A.; Galiano, H.; Lemordant, D.; Frackowiak, E.; Béguin, F.; Anouti, M. Triethylammonium Bis(tetrafluoromethylsulfonyl)amide Protic Ionic Liquid as An Electrolyte for Electrical Double-Layer Capacitors. *Phys. Chem. Chem. Phys.* **2012**, *14*, 8199−8207.
(27) Chaban, V. V.; Voroshylova, I. V.; Kalugin, O. N.; Prezhdo, O. V. Acetonitrile Boosts Conductivity of Imidazolium Ionic Liquids. *J. Phys. Chem. B* **2012**, *116*, 7719−7727.
(28) Takamuku, T.; Hoke, H.; Idrissi, A.; Marekha, B. A.; Moreau, M.; Honda, Y.; Umecky, T.; Shimomura, T. Microscopic Interactions of the Imidazolium-Based Ionic Liquid with Molecular Liquids Depending on Their Electron-Donicity. *Phys. Chem. Chem. Phys.* **2014**, *16*, 23627−23638.
(29) Kowsari, M. H.; Tohidifar, L. Tracing Dynamics, Self-Diffusion, and Nanoscale Structural Heterogeneity of Pure and Binary Mixtures of Ionic Liquid 1-Hexyl-2,3-dimethylimidazolium Bis(fluorosulfonyl)-imide with Acetonitrile: Insights from Molecular Dynamics Simulations. *J. Phys. Chem. B* **2016**, *120*, 10824−10838.
(30) Bardak, F.; Xiao, D.; Hines, L. G., Jr.; Son, P.; Bartsch, R. A.; Quitevis, E. L.; Yang, P.; Voth, G. A. Nanostructural Organization in Acetonitrile/Ionic Liquid Mixtures: Molecular Dynamics Simulations and Optical Kerr Effect Spectroscopy. *ChemPhysChem* **2012**, *13*, 1687−1700.
(31) Zheng, Y.-Z.; Wang, N.-N.; Luo, J.-J.; Zhou, Y.; Yu, Z.-W. Hydrogen-Bonding Interactions Between [BMIM][BF4] and Acetonitrile. *Phys. Chem. Chem. Phys.* **2013**, *15*, 18055−18064.
(32) Marekha, B. A.; Kalugin, O. N.; Bria, M.; Idrissi, A. Probing Structural Patterns of Ion Association and Solvation in Mixtures of Imidazolium Ionic Liquids with Acetonitrile by Means of Relative 1H and 13C NMR Chemical Shifts. *Phys. Chem. Chem. Phys.* **2015**, *17*, 23183−23194.
(33) Sun, S.; Zeng, H.; Robinson, D. B.; Raoux, S.; Rice, P. M.; Wang, S. X.; Li, G. Monodisperse MFe2O4 (M = Fe, Co, Mn) Nanoparticles. *J. Am. Chem. Soc.* **2004**, *126*, 273−279.
(34) Li, C.; Han, J.; Ryu, C. Y.; Benicewicz, B. C. A Versatile Method To Prepare RAFT Agent Anchored Substrates and the Preparation of PMMA Grafted Nanoparticles. *Macromolecules* **2006**, *39*, 3175−3183.
(35) Di Noto, V.; Vittadello, M.; Lavina, S.; Fauri, M.; Biscazzo, S. Mechanism of Ionic Conductivity in Poly(ethyleneglycol 400)/(LiCl)x Electrolytic Complexes: Studies Based on Electrical Spectroscopy. *J. Phys. Chem. B* **2001**, *105*, 4584−4595.
(36) Singh, M.; Odusanya, O.; Wilmes, G. M.; Eitouni, H. B.; Gomez, E. D.; Patel, A. J.; Chen, V. L.; Park, M. J.; Fragouli, P.; Iatrou, H.; Hadjichristidis, N.; Cookson, D.; Balsara, N. P. Effect of Molecular Weight on the Mechanical and Electrical Properties of Block Copolymer Electrolytes. *Macromolecules* **2007**, *40*, 4578−4585.
(37) Azuah, R. T.; Kneller, L. R.; Qiu, Y.; Tregenna-Piggott, P. L. W.; Brown, C. M.; Copley, J. R. D.; Dimeo, R. M. DAVE: A Comprehensive Software Suite for the Reduction, Visualization, and Analysis of Low Energy Neutron Spectroscopic Data. *J. Res. Natl. Inst. Stand. Technol.* **2009**, *114*, 341−358.
(38) Wittmar, A.; Ruiz-Abad, D.; Ulbricht, M. Dispersions of Silica Nanoparticles in Ionic Liquids Investigated with Advanced Rheology. *J. Nanopart. Res.* **2012**, *14*, 651.
(39) Hoarfrost, M. L.; Tyagi, M.; Segalman, R. A.; Reimer, J. A. Proton Hopping and Long-Range Transport in the Protic Ionic Liquid [Im][TFSI], Probed by Pulsed-Field Gradient NMR and Quasi-Elastic Neutron Scattering. *J. Phys. Chem. B* **2012**, *116*, 8201−8209.
(40) Chopade, S. A.; So, S.; Hillmyer, M. A.; Lodge, T. P. Anhydrous Proton Conducting Polymer Electrolyte Membranes via Polymerization-Induced Microphase Separation. *ACS Appl. Mater. Interfaces* **2016**, *8*, 6200−6210.
(41) Le, M. L. P.; Cointeaux, L.; Strobel, P.; Leprêtre, J.-C.; Judeinstein, P.; Alloin, F. Influence of Solvent Addition on the Properties of Ionic Liquids. *J. Phys. Chem. C* **2012**, *116*, 7712−7718.
(42) Liu, S.; Walton, M.; Tarakina, N. V.; Akcora, P. Solvation in Ionic Liquids with Polymer-Grafted Nanoparticles. *J. Phys. Chem. B* **2020**, *124*, 4843−4850.
(43) Aoun, B.; González, M. A.; Ollivier, J.; Russina, M.; Izaola, Z.; Price, D. L.; Saboungi, M.-L. Translational and Reorientational Dynamics of an Imidazolium-Based Ionic Liquid. *J. Phys. Chem. Lett.* **2010**, *1*, 2503−2507.

https://dx.doi.org/10.1021/acs.macromol.0c01434
Macromolecules 2020, 53, 6538−6546

(44) Singwi, K. S.; Sjölander, A. Diffusive Motions in Water and Cold Neutron Scattering. *Phys. Rev.* **1960**, *119*, 863−871.
(45) Burankova, T.; Hempelmann, R.; Fossog, V.; Ollivier, J.; Seydel, T.; Embs, J. P. Proton Diffusivity in the Protic Ionic Liquid Triethylammonium Triflate Probed by Quasielastic Neutron Scattering. *J. Phys. Chem. B* **2015**, *119*, 10643−10651.
(46) Fillion, J. J.; Brennecke, J. F. Viscosity of Ionic Liquid−Ionic Liquid Mixtures. *J. Chem. Eng. Data* **2017**, *62*, 1884−1901.
(47) Tariq, M.; Forte, P. A. S.; Gomes, M. F. C.; Lopes, J. N. C.; Rebelo, L. P. N. Densities and Refractive Indices of Imidazolium- and Phosphonium-Based Ionic Liquids: Effect of Temperature, Alkyl Chain Length, and Anion. *J. Chem. Thermodyn.* **2009**, *41*, 790−798.
(48) Susan, M. A. B. H.; Kaneko, T.; Noda, A.; Watanabe, M. Ion Gels Prepared by in Situ Radical Polymerization of Vinyl Monomers in an Ionic Liquid and Their Characterization as Polymer Electrolytes. *J. Am. Chem. Soc.* **2005**, *127*, 4976−4983.
(49) Kofu, M.; Someya, T.; Tatsumi, S.; Ueno, K.; Ueki, T.; Watanabe, M.; Matsunaga, T.; Shibayama, M.; Sakai, V. G.; Tyagi, M.; Yamamuro, O. Microscopic Insights Into Ion Gel Dynamics Using Neutron Spectroscopy. *Soft Matter* **2012**, *8*, 7888−7897.
(50) Ueno, K.; Inaba, A.; Kondoh, M.; Watanabe, M. Colloidal Stability of Bare and Polymer-Grafted Silica Nanoparticles in Ionic Liquids. *Langmuir* **2008**, *24*, 5253−5259.
(51) Ueno, K.; Sano, Y.; Inaba, A.; Kondoh, M.; Watanabe, M. Soft Glassy Colloidal Arrays in an Ionic Liquid: Colloidal Glass Transition, Ionic Transport, and Structural Color in Relation to Microstructure. *J. Phys. Chem. B* **2010**, *114*, 13095−13103.
(52) Ueno, K.; Fukai, T.; Nagatsuka, T.; Yasuda, T.; Watanabe, M. Solubility of Poly(methyl methacrylate) in Ionic Liquids in Relation to Solvent Parameters. *Langmuir* **2014**, *30*, 3228−3235.
(53) Bešter-Rogač, M.; Stoppa, A.; Hunger, J.; Hefter, G.; Buchner, R. Association of Ionic Liquids in Solution: a Combined Dielectric and Conductivity Study of [bmim][Cl] in Water and in Acetonitrile. *Phys. Chem. Chem. Phys.* **2011**, *13*, 17588−17598.

https://dx.doi.org/10.1021/acs.macromol.0c01434
Macromolecules 2020, 53, 6538−6546